Towards a load bearing hydrogel: A proof of principle in the use of osmotic pressure for biomimetic cartilage constructs

journal of the mechanical behavior of biomedical materials 137 (2023) 105552

Contents lists available at ScienceDirect

Journal of the Mechanical Behavior of Biomedical Materials

journal homepage: www.elsevier.com/locate/jmbbm

Towards a load bearing hydrogel: A proof of principle in the use of osmotic pressure for biomimetic cartilage constructs

Gerke H. Schuiringa, Maria Pastrama, Keita Ito, Corrinus C. van Donkelaar *

Orthopaedic Biomechanics, Dept. Biomedical Engineering, Eindhoven University of Technology, the Netherlands

A B S T R A C T

Cartilage defects occur frequently and can lead to osteoarthritis. Hydrogels are a promising regenerative strategy for treating such defects, using their ability of mimicking the native extracellular matrix. However, commonly used hydrogels for tissue regeneration are too soft to resist load-bearing in the joint. To overcome this, an implant is being developed in which the mechanical loadbearing function originates from the osmotic pressure generated by the swelling potential of a charged hydrogel, which is restricted from swelling by a textile spacer fabric. This study aims to quantify the relationship between the swelling potential of the hydrogel and the compressive stiffness of the implant.

Solutions with different molecular weight ratios of poly 2-hydroxyethyl methacrylate (pHEMA) and sodium methacrylate (NaMA) (20:0, 19:1, 18:2, 17:3) were used to create either plain hydrogels or HydroSpacers, which were obtained by injecting the hydrogel in a poly amide 6 (PA6) warp knitted spacer fabric. After equilibration in 0.15 M or 0.015 M sodium chloride solution, samples were mechanically tested in stress relaxation with a step deformation of 15% strain at a strain rate of 15% strain/sec and held till equilibrium was reached. Afterwards, samples were lyophilized to determine water, polymer content, fixed charge density (FCD) and osmotic pressure.

Hydrogels alone swelled up to 9-fold the initial weight, whereas HydroSpacers swelling was restricted to 1.2-fold. This restricted swelling of pHEMA-NaMA hydrogels in warp knitted PA6 spacer fabrics lead to an internal osmotic pressure. Regression analysis revealed a positive linear relationship between peak and equilibrium stress and osmotic pressure, showing that the mechanical properties of this so-called HydroSpacer can be tuned by adjusting the swelling capacity of the hydrogel via the FCD. In conclusion, a proof of principle is demonstrated using swelling hydrogels, where swelling of the hydrogel is restricted by the tension developing in the warp-knitted spacer fabric, resulted in a similar load-bearing mechanism as in healthy cartilage.

1. Introduction

There is a strong correlation between the load-bearing properties of articular cartilage and its total proteoglycan content (Kempson et al., 1970; X. Lux Lu et al., 2004; Lux Lu et al., 2007; Murakami et al., 2004). In healthy hydrated cartilage in the unloaded state, the solid matrix, especially the collagen fiber network, restricts the swelling originating from the Donnan osmotic pressure, which is caused by the ion imbalance between the bathing solution and the interstitial fluid due to the negative fixed charges of the proteoglycans (Grodzinsky et al., 1981; Kiviranta et al., 2006; Korhonen and Jurvelin, 2010; Maroudas, 1968, 1976; Maroudas and Bannon, 1981; Wilson et al., 2005). Moreover, the proteoglycan content provides both a high swelling pressure and a low hydraulic permeability, which results in a limited water loss during loading and fast recovery (Maroudas, 1976). The osmotic pressure, dependent on the fixed charge density (FCD) and osmolarity of the bathing solution, has been shown to be the dominating factor in the equilibrium response, contributing up to 50% of the equilibrium modulus (Korhonen et al., 2003; Xin L. Lu and Mow, 2008; Mow et al., 1998; Räsänen et al., 2017). By modulating the Donnan osmotic pressure using different external saline concentrations of the bathing solution, cartilage stiffness is affected, showing a 50% reduction of the equilibrium modulus when bathed in a hypertonic solution (Eisenberg and Grodzinsky, 1985; Korhonen and Jurvelin, 2010). When the tissue is depleted of proteoglycans, the modulus decreases to less than 2% of the original cartilage modulus (Guterl et al., 2010). Collagen, the other major component of the solid phase, is a crucial factor. The compressive stiffness of collagen is only significant at high compressive strains (Römgens et al., 2013). However, the specific arcade shaped and crosslinked collagen architecture in cartilage with fibers running from the cartilage-bone interface to the superficial layer (Benninghoff, 1925; Brown, Damen, and Thambyah, 2020), is essential for the generation of sufficient osmotic pressure by the encapsulated proteoglycan network. While the charged proteoglycans attract ions and therewith water, the

* Corresponding author. Eindhoven University of Technology, Dept. of Biomedical Engineering, Gem-Z 1.106, PO Box 513, 5600, MB Eindhoven the Netherlands.
E-mail address: c.c.v.donkelaar@tue.nl (C.C. van Donkelaar).

https://doi.org/10.1016/j.jmbbm.2022.105552
Received 13 September 2021; Received in revised form 27 October 2022; Accepted 31 October 2022
Available online 8 November 2022

tissue swells. This swelling tensions the collagen fibers, which then resist further swelling of the cartilage. Consequently, the number fixed charges per volume of water remains high, and therefore the osmotic pressure. Indeed, structural changes in collagen were shown to induce tissue swelling, suggesting failure to maintain the restricted swelling, leading to a decrease in stiffness of the tissue (Nickien et al., 2017). These results align with findings using a fibril-reinforced swelling poroviscoelastic model of articular cartilage (Wilson et al., 2004, 2005), where the equilibrium load was found to be predominantly carried by the osmotic swelling pressure, which finds its origin in restriction against swelling by the collagen fibers (Párraga Quiroga et al., 2017). In other words, the interaction between fluid, amorphous swelling proteoglycans and structured strain-resistant collagen fibers is essential for maintaining the mechanical properties and the load-bearing capacity of articular cartilage.

Due to trauma, focal cartilage defects may arise. Because cartilage has a limited capacity of self-regeneration, focal defects are often treated to prevent cartilage deterioration into osteoarthritis (OA). Current treatments of focal defects such as osteochondral autograft transfer, autologous chondrocyte implantation and microfracture do not lead to the desired outcomes, inducing fibrous tissue formation, opposing cartilage damage and donor site morbidity and are limited to specific age groups, lesion sites or sizes (Armiento et al., 2019; Magnussen et al., 2008). To address this, research pertaining to the development of regenerative implants for cartilage focal defects have resulted in a broad range of new methods and materials. Due to their ease of handling and mimicking the native cell environment, hydrogels are generally considered the most promising solution (Beddoes et al., 2016; Catoira et al., 2019; Xiao et al., 2013).

However, the poor load-bearing capacity of most hydrogels is one of the main hurdles in creating successful regenerative cartilage implants; only a few hydrogel formulations reach the lower range stiffnesses of native cartilage (Cook and Oyen, 2021; Tsou et al., 2016). To overcome this, fiber-reinforced hydrogels have been developed with significantly increased stiffness compared to hydrogels alone (Neves et al., 2020; Visser et al., 2015). In hydrogels that contain woven fibers, the weave architecture, yarn diameter and friction between yarns are the key role players for guiding stiffness, with smaller pore sizes and porosities and tighter weave architectures leading to an increased stiffness of the construct (Arjmandi et al., 2018; Moutos et al., 2016; Moutos, Freed, and Guilak, 2007a; Valonen et al., 2010). However, the addition of alginate, fibrin or agarose hydrogels did not increase the stiffness of the composite material in comparison with the woven construct alone (Liao et al., 2013; Moutos, Freed, and Guilak, 2007b). In contrast, hydrogel in a warp-knitted spacer fabrics, consisting of a knitted top and bottom layer which are connected by pile yarns, demonstrated a two to threefold increase of the Young's Modulus with non-swelling agarose or collagen-based hydrogels. Nevertheless, the Young's modulus of these spacer fabrics was still tenfold lower than of native cartilage (Schäfer et al., 2020). The present study postulates that using a swelling hydrogel in a warp-knitted spacer fabric would have superior load-bearing properties. In such construct, swelling of the hydrogel would be restricted by the tension developing in the warp-knitted spacer fabric, mimicking the restricted swelling of proteoglycans in the arcade-like collagen structure in healthy cartilage. This load-bearing mechanism is similar to that of healthy cartilage, which means that not only the equilibrium stiffness, but also peak stiffness and the time-dependent behavior may mimic that of cartilage. The properties of this so-called HydroSpacer can be tuned by adjusting the density of fixed negative charges in the gel, thus adjusting the swelling potential, or the properties of the spacer fabric, such as the stiffness of the fiber or the density of pile yarns. The objective of the present study is to demonstrate the potential of using non-regenerative HydroSpacers as load-bearing cartilage replacement material, and the effect of modulating the load-bearing capacity of the implant by tuning the swelling potential of the hydrogel.

2. Materials and methods

2.1. Spacer fabrics

Polyamide 6 (PA6) warp knitted spacer fabrics (Karl Mayer Textilmaschinenfabrik GmbH, Obertshausen, Germany) were used as restricting scaffold. The top and bottom layers were knitted using a multifilament yarn with a linear density of 44 dtex, applying 22.4 courses/cm and 37 wales/inch. The top and bottom parts were separated by a monofilament pile yarn with a linear density of 12 dtex, resulting in a total fabric height of 2.8 mm and fabric weight of 230.3 g/m^2. Samples of 8 mm diameter were cut from the spacer fabric using a laser cutter (VLS 3.50, Universal Laser Systems GmbH, Vienna, Austria). To visualize the macro- and microscopic morphology of the spacer fabric, a digital microscope (VHX-500F, Keyence Corporations, Osaka, Japan) was used.

2.2. Hydrogel

To create a hydrogel with adjustable swelling potential, 20 mol% 2-hydroxyethyl methacrylate (HEMA, Sigma-Aldrich St. Louis, MO, USA) sodium methacrylate (NaMA, Sigma-Aldrich, St. Louis, MO, USA) hydrogel was used, which was created with 79.98 mol% demi water, 0.01 mol% poly(ethylene glycol) dimethacrylate (DMPEG, Sigma-Aldrich, St. Louis, MO, USA) as crosslinker, and 0.01 mol% 2,2-azobis (2-methylpropionamide)dihydrochloride (Sigma-Aldrich, St. Louis, MO, USA) to initiate the polymerization.

The fixed charge density of the gel, determining its swelling potential, depends on the number of NaMA salt molecules that is incorporated in the copolymer. In the present study, four different compositions of the pHEMA:NaMA hydrogel were used in a 20:0, 19:1, 18:2 and 17:3 mol ratio. Unpolymerized hydrogel solution was stored at 4 °C and protected from light prior to use.

2.3. Hydrogel and HydroSpacer polymerization

Hydrogels and HydroSpacers were prepared in a custom-made Teflon mold system with chambers of 8 mm in diameter and 3 mm in height, connected by a channel. Spacer fabrics with equal diameter were weighted, inserted in the chambers and covered with a 1 mm thick glass slide (Corning Life Sciences, Tewksbury, USA). The hydrogel was injected using a syringe, while the mold was held in a vertical position. To ensure that no air bubbles were formed, CT imaging of representative samples was performed using a μCT100 imaging system (Scanco Medical, Brüttisellen, Swisterland), with voxelsize of 14.8 μm and energy level and intensity set to 45 kVp and 88 μA, respectively. The hydrogel was photopolymerized for 3 h at a distance of ~5 cm, using 4 UV lamps (Nailstar professional, London, UK) resulting in an intensity of 4.8 mW/cm^2 at a wavelength of 365 nm.

2.4. Swelling properties

2.4.1. Swelling ratio

To analyze the swelling potential of the hydrogels alone and in the HydroSpacers, the swelling ratio (SR, eq. (1)), FCD and osmotic pressure were calculated from the weights of the samples after bathing in a sodium chloride (NaCl) solution of 0.15 or 0.015 M until equilibrium was reached.

$$SR = \frac{m_{wet}}{m_0} \tag{1}$$

with m_0 and m_{wet} as the weight prior to and after swelling, respectively.

2.4.2. FCD

After the experiment, samples were lyophilized (Freezone 2.5, Lab-

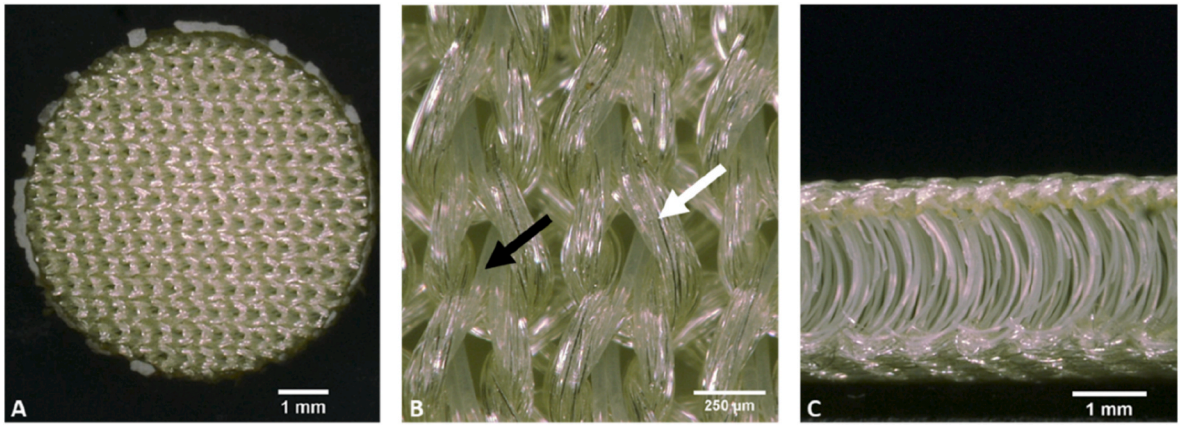

Fig. 1. Warp-knitted spacer fabric, without hydrogel. A) Top layer of the PA6 warp knitted spacer fabric. B) Close up of the warp knitted surface, with the multifilament indicated by the white arrow and the monofilament pile by the black arrow. C) Side view of the spacer fabric, with monofilaments separating the top and bottom layer.

conco, Kansas City, USA). The water content and polymer content were determined by subtracting the dry weight from the wet weight and by subtracting the weight of the spacer fabric from the dry weight, respectively (eqs (2) and (3)).

$$m_{H_2O} = m_{wet} - m_{dry} \tag{2}$$

$$m_P = m_{dry} - m_{spacer\ fabric} \tag{3}$$

Using the NaMA density of the gel and polymer mass present in the HydroSpacer, the FCD of the constructs was obtained (eq (4)) (Han et al., 2011).

$$FCD = \frac{m_{NaMA} * \left(\frac{z_{NaMA}}{MW_{NaMA}}\right)}{m_{H_2O}} * \frac{1000\ mEq}{mol - charge} \tag{4}$$

with FCD in mEq/g, m_{NaMA} and m_{H_2O} respectively the mass of NaMA and total water content in mg, z_{NaMA} the mol-charge and MW_{NaMA} the molecular weight of NaMA.

2.4.3. Osmotic pressure

From the FCD, the osmotic pressure difference produced by the interactions of the bathing solution and the FCD was calculated (eq (5)) (X. Lux Lu et al., 2004).

$$\Delta\pi = \pi_{intern} - \pi_{extern} = RT\left(\sqrt{c^{F2} + 4c^{*2}} - 2c^*\right) \tag{5}$$

with R the gas constant, T the absolute temperature, c^F the FCD and c* the osmolarity of the bathing solution.

2.5. Mechanical properties

To investigate the mechanical effect of the osmotic pressure on the constructs, a confined compression test was performed using a tensile tester (Model 42, MTS Criterion, Eden Prairie, USA) equipped with a loadcell of 5 kN (LSB.503, MTS systems corp., Eden Prairie, USA). After polymerization, the samples were placed in a custom-made stainless-steel confined set-up with a diameter of 8 mm. A porous platen (316L stainless steel with 200 µm pore size, THN, Enschede, Netherlands), a custom-made piston and a 7 mm diameter stainless steel ball (Fabory, Tilburg, Netherlands) were placed consecutively on top of the sample, to allow fluid flow throughout the test (Fig. 2). Subsequently, the bathing solution was added to the container and the construct was allowed to swell for ~24 h while a constant preload of 50 kPa was applied to keep the specimen in place. After the maximum height of the construct was reached, the crosshead position was fixed, and the swelling pressure induced by the construct was allowed to equilibrate prior to further testing.

To determine the mechanical properties, a stress relaxation test was performed by applying 15% strain, relative to the equilibrium height after swelling, with a strain rate of 15%/sec. The strain was held constant for 2.5 h and stress relaxation was measured at a frequency of 10 Hz. The peak and equilibrium stresses (σ_t and σ_{Eq}), were calculated from the relaxation curve. To obtain the fast and slow relaxation response (τ_1 and τ_2), Matlab (Mathworks Inc., Natick, Massachusetts, United States) curve fitting was used (eq (6)).

$$\sigma_t = a + b^{(-t/\tau_1)} + c^{(-t/\tau_2)} \tag{6}$$

where t is the test time in seconds and a and b are constants.

To calculate the hydraulic permeability k, equation (7) previously described by Cutcliffe and Defrate (2020) was used.

$$k = \frac{h^2}{H_A \tau_2} \tag{7}$$

where h is the height of the sample after swelling and H_A the aggregate modulus at 15% strain.

2.6. Statistical analysis

Data are presented as mean ± standard deviation. A two-way ANOVA with Tukey's multiple comparison post-hoc testing was used to compare the effect of hydrogel composition and bathing solution on the swelling and mechanical properties. A multiple linear regression model was applied to determine the effects of the dependent variables on peak and equilibrium stress. All analyses were performed using Prism GraphPad. A p-value < 0.05 was indicated as significant difference between groups (*p < 0.05, **p < 0.01, ***p < 0.001).

3. Results

3.1. Swelling, FCD and osmotic pressure

Plain hydrogels (Fig. 3A and B and left pairs of columns in Fig. 4) swell up to 8.8 times their original volume (Fig. 4A). Significant increase in swelling was found with increasing initial density of fixed charges (NaMA content), and with lower concentration of external saline concentration (0.15 vs 0.015 M NaCl), in agreement with osmotic swelling theories (Fig. 4A). All HydroSpacers (Fig. 3D and E and right pair of columns in Fig. 4) containing NaMA swelled 1.2 times, independent of NaMA density or saline concentration of the bathing solution (Fig. 4A).

With more swelling, the charges in the polymer network are diluted in a larger volume of water. Consequently, the effective FCD (mEq/L)

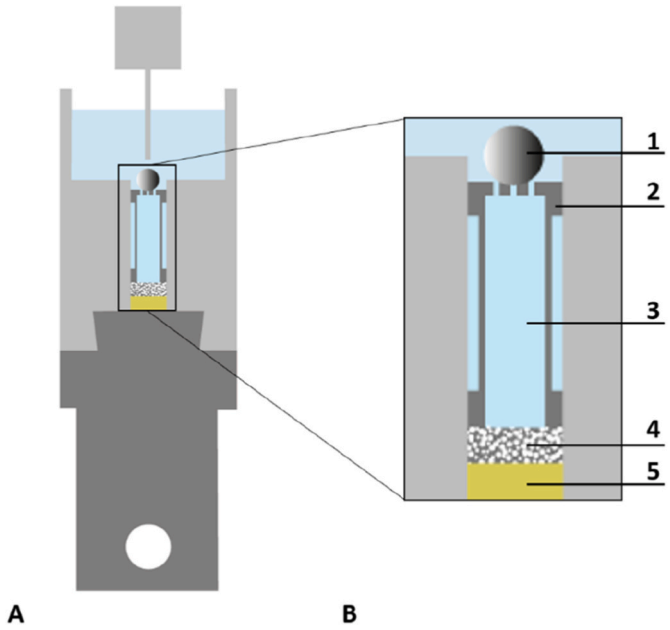

Fig. 2. Confined test set-up, consisting of a stainless-steel confined chamber containing the bathing solution, with the lower part mounted on the tensile tester (A) and the upper part containing ball on top (1), piston (2), bathing solution (3) porous platen (4) and the sample (5) (B).

and the osmotic pressure in equilibrium was similar between hydrogels (Fig. 4B and C). With similar water uptake, yet different density of fixed negative charges incorporated in the polymer, the effective FCD in equilibrium of HydroSpacers significantly increased with increasing NaMA concentration up to 0.8 mEq/mg in the 17:3 composition (Fig. 4B).

The hydrogels in 0.015 M NaCl develop slightly higher osmotic pressure compared to those in 0.15 M NaCl (Fig. 4C), because stresses develop in the crosslinked polymeric network when it swells, and these stresses resist further swelling. For HydroSpacers, the lowest osmotic pressure can apparently stretch the pile yarns till 20% strain, but the highest osmotic pressures are unable to stretch the pile yarns much more than that. This may be explained by the bended structure of the pile yarns after warp-knitting (Figs. 1C and 3C,D). During swelling until 1.2 times the original height, the pile yarns straighten (Fig. 3E). Further swelling would strain the PA6 fibers, but the combination of all PA6 pile yarns is stiff enough to restrict swelling even for the case with the highest osmotic pressure. Consequently, there is also a significant difference in osmotic swelling pressure depending on the amount of NaMA and on the bathing solution (eq (5), Fig. 4C). CT images confirmed there were no air bubbles present in the HydroSpacers (Fig. 3F).

3.2. Mechanical properties of the HydroSpacer constructs

With increasing NaMA concentration, the peak stress increased significantly for all HydroSpacer groups. For the equilibrium stress, significant differences were found between all groups in comparison with the 17:3 composition, for both bathing solutions. In contrast to the calculated osmotic pressures (Fig. 4C), no significant differences were found in the stresses of the HydroSpacer consisting of the same hydrogel composition in the different bathing solutions. Theoretically it should be larger, following the osmotic pressure, and although the trend is clear, there is no significant difference (Fig. 5).

A multiple linear regression was performed with the dependent variables water content (w%), polymer content (w%), osmotic pressure (kPa), and bathing solution osmolarity (M), to identify the variables that have a significant influence on the measured peak and equilibrium stress. Only the osmotic pressure had a significant effect on both stresses, whereas the composition does not significantly influence the outcome (Table 1).

Further linear regression analysis revealed a significant linear relationship between osmotic pressure and peak (Fig. 6A) and equilibrium stresses (Fig. 6B) in HydroSpacers, with a R^2 of 0.48 and 0.69, respectively.

Moreover, a non-linear relationship between hydraulic permeability and FCD was observed, indicating that the hydraulic permeability decreased with an increased FCD, which was shown for both groups bathed in 0.15 M NaCl and 0.015 M NaCl ($R^2 = 0.62$ and 0.51, respectively, Fig. 7).

4. Discussion

This study demonstrates that HydroSpacers containing hydrogels with incorporated fixed negative charges have equilibrium stiffness (1–4 MPa), peak stress (10–30 MPa) and permeability (10^{-15}-10^{-16} m^4/Ms) very similar to healthy articular cartilage (Figs. 5 and 7). This load-bearing principle is identical to that in native cartilage, in which the load-bearing properties originate from the osmotic pressure induced by the FCD of the proteoglycan network and the restricting collagen network (Párraga Quiroga et al., 2017). The relationship between these

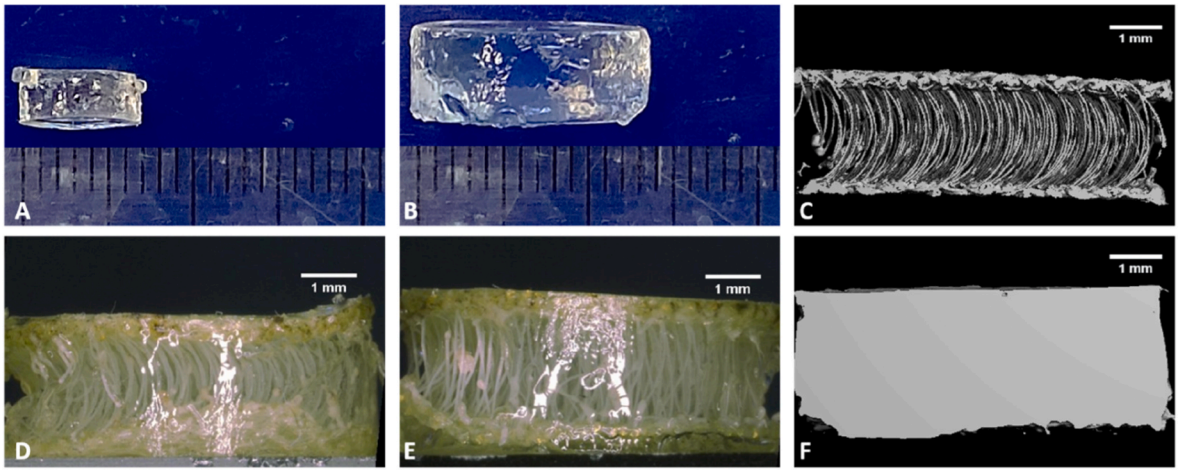

Fig. 3. pHEMA: NaMA hydrogel with a 17:3 composition prior (A) and after swelling (B) in 0.15M NaCl. A difference in stretching of the pile yarns was observed in HydroSpacers directly prior (D) and after swelling (E). To confirm no air bubbles were present μCT images were taken from the construct, with an empty PA6 spacer fabric (C) and injected with pHEMA (F).

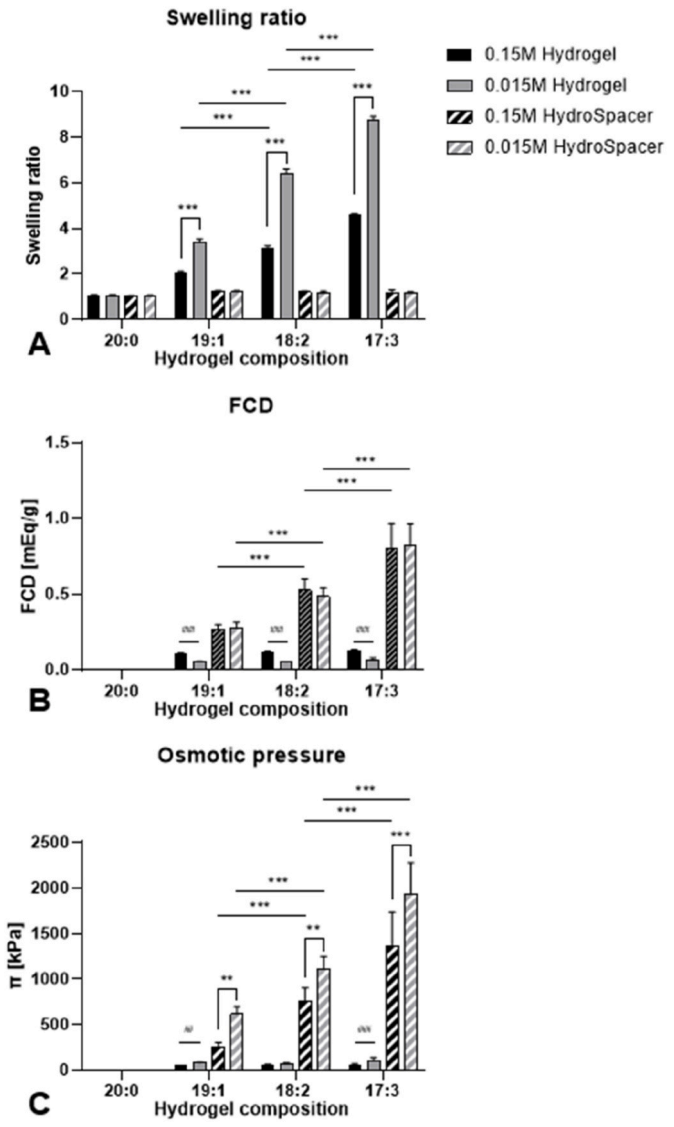

Fig. 4. Swelling ratios (A), FCDs (B) and osmotic pressures (C) of the four pHEMA-NaMA hydrogel compositions used, without and with the fiber reinforcement of a PA6 spacer fabric (HydroSpacer) bathed in 0.15M or 0.015M NaCl.

variables and the osmotic pressure illustrates that the mechanical properties of a HydroSpacer constructs can be tuned over a wide range by changing the FCD. Similar to cartilage (Chahine et al., 2005; Chen et al., 2001; Lux Lu et al., 2007; Nickien et al., 2017), FCD and external salt concentration in the bathing solution together determine the mechanical properties of the HydroSpacers (Fig. 4B). Though the osmotic pressure increases with a decreased salt concentration of the bathing solution (Fig. 4C), this did not lead to significant differences of the peak and equilibrium stresses between groups with the same pHEMA:NaMA composition and FCD 0.3–1.0 mEq/mL (Fig. 5). Similarly, in cartilage with FCDs of 0.3–0.4 mEq/mL the apparent Young's modulus plateaued with bathing solutions between 0.15 M and 0.015 M NaCl (Lux Lu et al., 2007). Finally, the reverse relationship between the FCD and the hydraulic permeability in cartilage (Gu et al., 1993; Maroudas, 1968) was also apparent in the HydroSpacers (Fig. 7).

Although in the study of Schäfer et al. a significant increase of the Young's Modulus was observed with the introduction of hydrogels in warp-knitted poly (ethylene terephthalate) spacer fabrics compared to empty warp-knitted spacer fabrics, native cartilage stiffnesses were not reached (Schäfer et al., 2020). The same applies for the use of chitosan nanofibers as fiber reinforced material in swelling hydrogels. By inserting nanofibers, swelling of polyacrylamide hydrogels was reduced by 75%, but a distinct difference in sustained stress between the restricted and free swelling hydrogel only occurred at non-physiological strain levels higher than 60% (Sanchez-Adams et al., 2014; Zhou and Wu, 2011). Restricted swelling up to 90% of three hydrogel compositions in woven poly(ε-caprolactone) (PCL) scaffolds led to an approximately 10-fold increase of the equilibrium modulus. The degree to which the swelling was restricted correlated with the increase in equilibrium modulus (Moffat et al., 2018).

This is in line with the results shown in the present study, in which peak and equilibrium stress both depend on the amount of restricted swelling. In the study of Moffat et al., swelling hydrogels could increase volume even when restricted in fiber meshes, which was not possible in the PA6 spacer fabrics in the present study (Fig. 3A). Apparently, the present fibers were stiffer or the pile yarns were denser. As a result of their swelling, Moffat's equilibrium moduli were less dependent on

Table 1
Multiple linear regression analysis between peak or equilibrium stress, and water content, polymer content, bathing solution or osmotic pressure.

	Bathing solution	Adjusted R squared	Osmotic pressure	Water content (w%)	Polymer content (w %)
Peak stress	0.15M NaCl	0.8103	<0.001 (***)	0.070 (ns)	0.133 (ns)
	0.015M NaCl	0.8607	<0.001 (***)	0.412 (ns)	0.613 (ns)
Equilibrium stress	0.15M NaCl	0.666	<0.001 (***)	0.545 (ns)	0.442 (ns)
	0.015M NaCl	0.734	<0.001 (***)	0.252 (ns)	0.205 (ns)

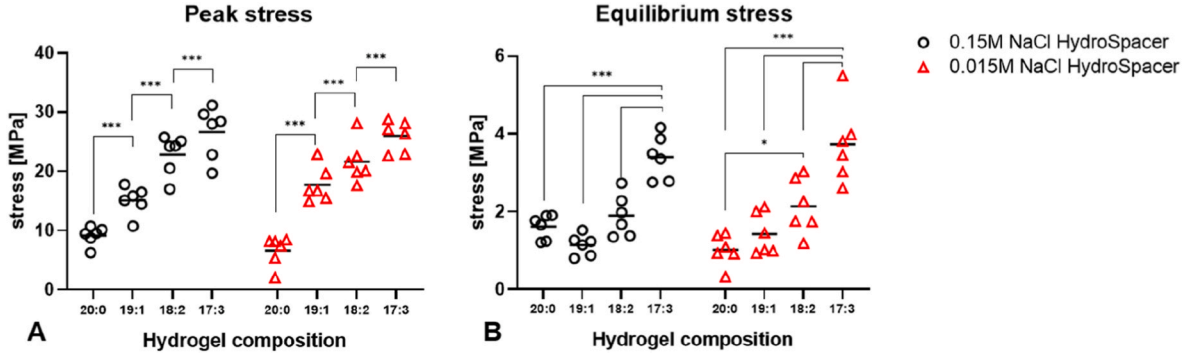

Fig. 5. Peak (A) and equilibrium (B) stress at 15% strain for HydroSpacers. Significant differences can be found with an increased NaMA concentration and is not dependent on bathing solution.

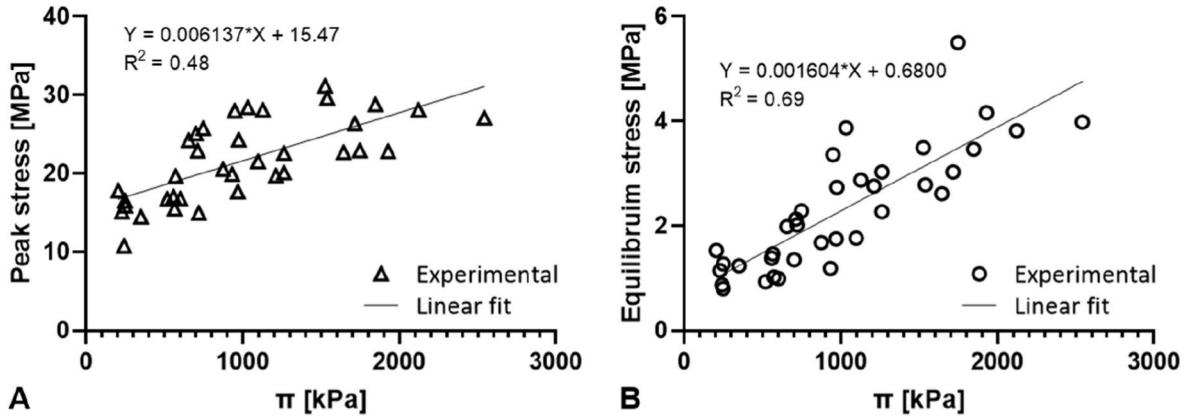

Fig. 6. Regression model of the peak and equilibrium stress as a function of osmotic pressure.

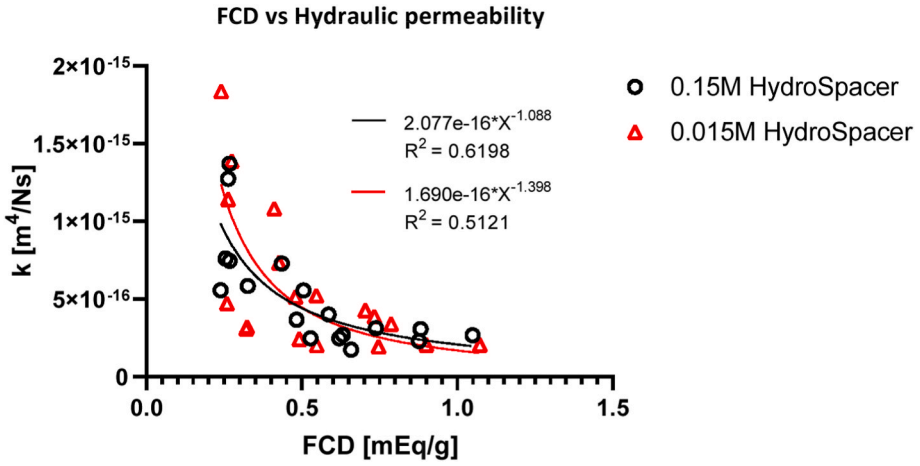

Fig. 7. Calculated values of the hydraulic permeability plotted against the FCD. The fitted line shows a non-linear relationship between the FCD and the hydraulic permeability for both bathing solutions.

hydrogel compositions than the fully restricted HydroSpacers in the current study (Fig. 5B) (Moffat et al., 2018). With changing the spacer fabric material, the stiffness of the pile yarns is the key factor for the stiffness of the whole construct. Using stiffer pile yarns, less swelling is allowed resulting in higher stiffnesses using the same hydrogel and vice versa. However, different spacer fabric materials might also alter the properties of the hydrogel, e.g. through chemical reactions with the hydrogel, alterations in cross-linking during the polymerization process, etc.

Restricted swelling results in high FCD and osmotic pressure, mimicking the interaction between proteoglycans and collagen in native cartilage tissue. Cartilage swelling correlates with collagen degradation in osteoarthritic cartilage (Bank et al., 2000). Indeed, intact cartilage tissue detached from the bone swells 12% in 0.15M NaCl, while degenerate cartilage swells up to 51% (Nickien et al., 2017). This shows the importance of an intact collagen network to withstand the internal swelling pressure. In healthy cartilage, collagen in the deep zone is thought to be strained by 2–3% (Schinagl et al., 1997; Wilson et al., 2004).

In native tissue, the FCD ranges from 0.04 to 0.3 mEq/mL (Chen et al., 2001; Korhonen et al., 2003). The FCD in 19:1 pHEMA:NaMA hydrogel (0.27 mEq/g) is within this range, but the calculated FCDs in the other two hydrogel compositions is larger. Reported osmotic pressures increase with increasing FCD in cartilage and hydrogels. Cartilage with FCD between 0.08 and 0.18 mEq/mL has osmotic pressures up to 200 kPa in 0.015 M NaCl (Chen et al., 2001), the 0.27 mEq/mL 19:1 HydroSpacer in the present study reaches 250 kPa and 615 kPa in 0.15M and 0.015M NaCl, respectively (Fig. 4B). Chondroitin sulfate (CS) solutions with an FCD of 0.5 mEq/mL reach 0.42 MPa and 0.6 MPa in 0.15 M and 0.015 M NaCl solutions, respectively (Chahine et al., 2005). This FCD is comparable with that of 18:2 pHEMA:NaMA HydroSpacers, which reach in 0.15M NaCL 0.75 MPa osmotic pressures. Hydrogels with FCD 0.8 mEq/mL reach approximately 1.3 MPa osmotic pressure in a physiological solution (Han et al., 2011), similar to the 17:3 pHEMA: NaMA HydroSpacer.

Spacer fabrics restrict swelling in the 17:3–0.015 M NaCl group 8.8/1.2 = 7.3-fold, resulting in an 2000/100 = 20-fold increase in internal osmotic pressure. With the osmotic pressure taking 90% of the load bearing capacity in equilibrium (Párraga Quiroga et al., 2017), the load bearing capacity of the HydroSpacer is 0.9*20 = 18 times increased. With the equilibrium modulus of native cartilage ranging between 0.1 and 2 MPa (Little et al., 2011) at 15% strain, this 90% would give estimated osmotic pressures between 13 kPa and 270 kPa, comparable to the osmotic pressure values found in HydroSpacers with the 19:1 composition (250 kPa).

Finally, permeability in HydroSpacers with the lower FCDs correspond with values of native cartilage (10^{-16}-10^{-15} m^4/Ms) (Little et al., 2011).

In this study, 2.8 mm high PA6 fabrics were used, which is in the high range of tibia plateau cartilage thickness (Shepherd and Seedhom, 1999). The mechanical performance will be independent of samples size, as it is determined by the fixed charge density in the tissue, which is determined by gel composition and swelling, which is equal throughout samples. There are some major advantages of using cartilage-implants

based on swelling hydrogels in which the swelling is restricted by a fiber mesh. First, they are immediately load-bearing even without neotissue formation by seeded chondrocytes. Typically, (M)ACI-type surgeries with cell-seeded gels are too soft for load-bearing immediately post-operatively. These constructs develop stiffness over time when matrix is being produced by the cells. Therefore, a significant period of non-loading is required after surgery(Edwards et al., 2014). This is not needed with HydroSpacers, as these constructs are immediately load-bearing due to their inherent osmotic pressure. Second, HydroSpacers have cartilage-mimicking mechanical properties, which means that their surface is pliable. This provides these implants with an advantage over clinically used metal resurfacing implants, which are very stiff and may consequently damage opposing cartilage, in particular when implanted at a slight angle (Diermeier et al., 2020; Heuijerjans et al., 2018). Another advantage of HydroSpacers over metal implants is that MRI remains possible. The spacer fabric and hydrogel materials used in this paper were chosen based on their reproducible properties, to demonstrate the proof of principle. In other versions, biocompatible spacer fabric (eg PCL-based) and hydrogels (eg Chondroitin sulfate-based) may be used, which allows this system to be used as a regenerative platform (Levett et al., 2014; Schuurmans et al., 2021). Ultimately, creating an osteochondral implant by combining a regenerative HydroSpacer adhered to a synthetic bone scaffold is desired to induce osteointegration and stabilization, which will be in the end beneficial for the treatment of osteochondral defects caused by for example trauma or osteochondritis dissecans in younger and active patients, as it allows patients to instantly load the affected joint and reduce recovery times.

In conclusion, this study is the proof of principle that it is possible to mimic the load-bearing mechanism in cartilage by injecting a swelling hydrogel in a strain-limiting spacer fabric. The positive linear relationship between peak and equilibrium stress and osmotic pressure allow the mechanical properties of this so-called HydroSpacer to be tuned by adjusting the swelling capacity of the hydrogel via the FCD. In this study non-regenerative materials were used. In the future, cell-seeded biocompatible and biodegradable swelling hydrogels may be used in combination with biocompatible warp-knitted spacers fabrics to create regenerative implants with immediate load-bearing properties.

CRediT authorship contribution statement

Gerke H. Schuiringa: Conceptualization, Data curation, Formal analysis, Investigation, Methodology, Visualization, Writing – original draft, Writing – review & editing. **Maria Pastrama:** Writing – review & editing. **Keita Ito:** Conceptualization, Funding acquisition, Supervision, Writing – review & editing. **Corrinus C. van Donkelaar:** Conceptualization, Supervision, Writing – review & editing.

Declaration of competing interest

The authors declare that they have no known competing financial interests or personal relationships that could have appeared to influence the work reported in this paper.

Data availability

Data will be made available on request.

Acknowledgements

This research was performed under the framework of Chemelot InSciTe, supported by the partners of Regenerative Medicine Crossing Borders and powered by Health~Holland, Top Sector Life Sciences & Health.

References

Arjmandi, Mohammadreza, et al., 2018. Mechanical and tribological properties of a novel hydrogel composite reinforced by three-dimensional woven textiles as a functional synthetic cartilage. Compos. Appl. Sci. Manuf. 115, 123–133. https://linkinghub.elsevier.com/retrieve/pii/S1359835X18303762.

Armiento, Angela R., Alini, Mauro, Stoddart, Martin J., 2019. Articular fibrocartilage - why does hyaline cartilage fail to repair? Adv. Drug Deliv. Rev. 146, 289–305. https://linkinghub.elsevier.com/retrieve/pii/S0169409X18303193. (Accessed 12 May 2021).

Bank, Ruud A., Soudry, Michael, Maroudas, Alice, Mizrahi, Joseph, Tekoppele, Johan M., Bank, 2000. The increased swelling and instantaneous deformation of osteoarthritic cartilage is highly correlated with collagen degradation. Arthritis Rheum. 43 (10), 2202–2210. https://pubmed.ncbi.nlm.nih.gov/11037879/. (Accessed 5 August 2021).

Beddoes, Charlotte M., Whitehouse, Michael R., Briscoe, Wuge H., Su, Bo, 2016. Hydrogels as a replacement material for damaged articular hyaline cartilage. Materials 9 (6).

Benninghoff, A., 1925. Form und bau der gelenkknorpel in ihren beziehungen zur funktion - zweiter teil: der aufbau des gelenkknorpels in seinen beziehungen zur funktion. Z. für Zellforsch. Mikrosk. Anat. 2 (5), 783–862. https://link.springer.com/article/10.1007/BF00583443. (Accessed 4 August 2021).

Brown, Emma Te, Tümanako, Alicia Helena, Antonetta Damen, Thambyah, Ashvin, 2020. The mechanical significance of the zonally differentiated collagen network of articular cartilage in relation to tissue swelling. Clin. BioMech. 79, 104926.

Catoira, Marta Calvo, et al., 2019. Overview of natural hydrogels for regenerative medicine applications. J. Mater. Sci. Mater. Med. 30 (10), 1–10.

Chahine, Nadeen O., Chen, Faye H., Hung, Clark T., Ateshian, Gerard A., 2005. Direct measurement of osmotic pressure of glycosaminoglycan solutions by membrane osmometry at room temperature. Biophys. J. 89 (3), 1543–1550.

Chen, S.S., et al., 2001. Depth-dependent compressive properties of normal aged human femoral head articular cartilage: relationship to fixed charge density. Osteoarthritis Cartilage 9 (6), 561–569. https://www.sciencedirect.com/science/article/pii/S1063458401904248?via%3Dihub. (Accessed 23 August 2019).

Cook, Robert F., Oyen, Michelle L., 2021. On the failure and fracture of hydrogels for cartilage replacement. J. Phys. Mater 4, 21001. https://doi.org/10.1088/2515-7639/abdb39.

Cutcliffe, Hattie C., Defrate, Louis E., 2020. Comparison of Cartilage Mechanical Properties Measured during Creep and Recovery. https://doi.org/10.1038/s41598-020-58220-2.

Diermeier, Theresa, et al., 2020. Effects of focal metallic implants on opposing cartilage - an in-vitro study with an abrasion test machine. BMC Muscoskel. Disord. 21 (1), 261. https://bmcmusculoskeletdisord.biomedcentral.com/articles/10.1186/s12891-020-03292-4. (Accessed 16 December 2021).

Edwards, Peter K., Ackland, Timothy, Ebert, Jay R., 2014. Clinical rehabilitation guidelines for matrix-induced autologous chondrocyte implantation on the tibiofemoral joint. J. Orthop. Sports Phys. Ther. 102 (2), 102–119. www.jospt.org. (Accessed 16 December 2021).

Eisenberg, Solomon R., Grodzinsky, Alan J., 1985. Swelling of articular cartilage and other connective tissues: electromechanochemical forces. J. Orthop. Res. 3 (2), 148–159, 10.1002/jor.1100030204.

Grodzinsky, A.J., Roth, V., Myers, E., Grossman, W.D., Mow, V.C., 1981. The significance of electromechanical and osmotic forces in the nonequilibrium swelling behavior of articular cartilage in tension. J. Biomech. Eng. 103 (4), 221–231.

Gu, W.Y., Lai, W.M., Mow, V.C., 1993. Transport of fluid and ions through a porous-permeable charged-hydrated tissue, and streaming potential Data on normal bovine articular cartilage. J. Biomech. 26 (6), 709–723.

Guterl, Canal, Clare, Clark T. Hung, Ateshian, Gerard A., 2010. Electrostatic and non-electrostatic contributions of proteoglycans to the compressive equilibrium modulus of bovine articular cartilage. J. Biomech. 43 (7), 1343–1350.

Han, EunHee, Chen, Silvia S., Klisch, Stephen M., Sah, Robert L., 2011. Contribution of proteoglycan osmotic swelling pressure to the compressive properties of articular cartilage. Biophys. J. 101 (4), 916–924. https://www.sciencedirect.com/science/article/pii/S0006349511008344#%FE%FF%00a%00p%00p%002. (Accessed 30 October 2018).

Heuijerjans, Ashley, Wilson, Wouter, Ito, Keita, Corrinus, C., van Donkelaar, 2018. Osteochondral resurfacing implantation angle is more important than implant material stiffness. J. Orthop. Res. 36 (11), 2911–2922. https://pubmed.ncbi.nlm.nih.gov/29943463/. (Accessed 16 December 2021).

Kempson, G.E., Helen Muir, S.A.V., Swanson, Freemas, M.A.R., 1970. Correlations between stiffness and the chemical constituents of cartilage on the human femoral head. Biochim. Biophys. Acta Mol. Cell Res. 215, 70–77.

Kiviranta, Panu, et al., 2006. Collagen network primarily controls Poisson's ratio of bovine articular cartilage in compression. J. Orthop. Res. 24 (4), 690–699, 10.1002/jor.20107. (Accessed 19 December 2018).

Korhonen, Rami K., Jurvelin, Jukka S., 2010. Compressive and tensile properties of articular cartilage in axial loading are modulated differently by osmotic environment. Med. Eng. Phys. 32 (2), 155–160. https://linkinghub.elsevier.com/retrieve/pii/S1350453309002367.

Korhonen, Rami K., et al., 2003. Fibril reinforced poroelastic model predicts specifically mechanical behavior of normal, proteoglycan depleted and collagen degraded articular cartilage. J. Biomech. 36 (9), 1373–1379.

Levett, Peter A., et al., 2014. A biomimetic extracellular matrix for cartilage tissue engineering centered on photocurable gelatin, hyaluronic acid and Chondroitin sulfate. Acta Biomater. 10 (1), 214–223. https://www.sciencedirect.com/science/article/pii/S1742706113005138?via%3Dihub. (Accessed 27 November 2019).

Liao, I. Chien, et al., 2013. Composite three-dimensional woven scaffolds with interpenetrating network hydrogels to create functional synthetic articular cartilage. Adv. Funct. Mater. 23 (47), 5833–5839, 10.1002/adfm.201300483.
Lu, Xin L., Mow, Van C., 2008. Biomechanics of articular cartilage and determination of material properties. Med. Sci. Sports Exerc. 40 (2), 193–199.
Little, Christopher James, Bawolin, Nahshon Kenneth, Chen, Xiongbiao, 2011. Mechanical properties of natural cartilage and tissue-engineered constructs. Tissue Eng. B Rev. 17 (4), 213–227. http://www.liebertonline.com/doi/abs/10.1089/ten.teb.2010.0572.
Lu, X. Lux, et al., 2004. Indentation determined mechanoelectrochemical properties and fixed charge density of articular cartilage. Ann. Biomed. Eng. 32 (3), 370–379.
Lux Lu, X., et al., 2007. The generalized triphasic correspondence principle for simultaneous determination of the mechanical properties and proteoglycan content of articular cartilage by indentation. J. Biomech. 40 (11), 2434–2441. https://wwwsciencedirectcom/science/article/pii/S0021929006004532?via%3Dihub#fig2. (Accessed 30 October 2018).
Magnussen, Robert A., Dunn, Warren R., Carey, James L., Spindler, Kurt P., 2008. Treatment of focal articular cartilage defects in the knee: a systematic review. Clin. Orthop. Relat. Res. 466 (4), 952–962. /pmc/articles/PMC2504649/(May 18, 2021).
Maroudas, A., 1968. Physicochemical properties of cartilage in the light of ion exchange theory. Biophys. J. 8 (5), 575–595.
Maroudas, A., 1976. Balance between swelling pressure and collagen tension in normal and degenerate cartilage. Nature 260 (5554), 808–809.
Maroudas, A., Bannon, C., 1981. Measurement of swelling pressure in cartilage and comparison with the osmotic pressure of constituent proteoglycans. Biorheology 18 (3–6), 619–632.
Moffat, Kristen L., et al., 2018. Composite cellularized structures created from an interpenetrating polymer network hydrogel reinforced by a 3D woven scaffold. Macromol. Biosci. 18 (10), 1800140, 10.1002/mabi.201800140.
Moutos, Franklin T., Freed, Lisa E., Guilak, Farshid, 2007a. A biomimetic three-dimensional woven composite scaffold for functional tissue engineering of cartilage. Nat. Mater. 6 (2), 162–167.
Moutos, Franklin T., Freed, Lisa E., Guilak, Farshid, 2007b. A biomimetic three-dimensional woven composite scaffold for functional tissue engineering of cartilage. Nat. Mater. 6, 162–167. https://doi.org/10.1038/nmat1822.
Moutos, Franklin T., Glass, Katherine A., Compton, Sarah A., Ross, Alison K., Gersbach, Charles A., Guilak, Farshid, Estes, Bradley T., 2016. Anatomically shaped tissue-engineered cartilage with tunable and inducible anticytokine delivery for biological joint resurfacing. Proc. Natl. Acad. Sci. USA 113 (31), E4513–E4522. http://www.pnas.org/lookup/doi/10.1073/pnas.1601639113.
Mow, V.C., Ateshian, G.A., Lai, W.M., Gu, W.Y., 1998. Effects of fixed charges on the stress-relaxation behavior of hydrated soft tissues in a confined compression problem. Int. J. Solid Struct. 35 (34–35), 4945–4962.
Murakami, T., et al., 2004. Influence of proteoglycan on time-dependent mechanical behaviors of articular cartilage under constant total compressive deformation. JSME Int. J. Ser. C. 47 (4), 1049–1055. http://www.jstage.jst.go.jp/article/jsmec/47/4/47_4_1049/_article.
Neves, Sara C., Moroni, Lorenzo, Barrias, Cristina C., Granja, Pedro L., 2020. Leveling up hydrogels: hybrid systems in tissue engineering. Trends Biotechnol. 38 (3), 292–315. https://doi.org/10.1016/j.tibtech.2019.09.004.
Nickien, Mieke, Thambyah, Ashvin, Broom, Neil D., 2017. How a decreased fibrillar interconnectivity influences stiffness and swelling properties during early cartilage degeneration. J. Mech. Behav. Biomed. Mater. 75, 390–398. https://www.sciencedirect.com/science/article/pii/S1751616117303259?via%3Dihub. (Accessed 30 October 2018).
Párraga Quiroga, J.M., Wilson, W., Ito, K., van Donkelaar, C.C., 2017. Relative contribution of articular cartilage's constitutive components to load support depending on strain rate. Biomech. Model. Mechanobiol. 16 (1), 151–158. http://link.springer.com/10.1007/s10237-016-0807-0.
Räsänen, Lasse P., et al., 2017. The effect of fixed charge density and cartilage swelling on mechanics of knee joint cartilage during simulated gait. J. Biomech. 61, 34–44.
Römgens, Anne M., Van Donkelaar, Corrinus C., Ito, Keita, 2013. Contribution of collagen fibers to the compressive stiffness of cartilaginous tissues. Biomech. Model. Mechanobiol. 12 (6), 1221–1231.
Sanchez-Adams, Johannah, et al., 2014. The mechanobiology of articular cartilage: bearing the burden of osteoarthritis. Curr. Rheumatol. Rep. 16 (10), 1–9. /pmc/articles/PMC4682660/(April 10, 2021).
Schäfer, Benedikt, et al., 2020. Warp-knitted spacer fabrics: a versatile platform to generate fiber-reinforced hydrogels for 3D tissue engineering. Materials 13 (16). https://pubmed.ncbi.nlm.nih.gov/32785204/. (Accessed 24 February 2021).
Schinagl, Robert M., Gurskis, Donnell, Chen, Albert C., Sah, Robert L., 1997. Depth-dependent confined compression modulus of full-thickness bovine articular cartilage. J. Orthop. Res. 15 (4), 499–506. https://onlinelibrary.wiley.com/doi/10.1002/jor.1100150404. (Accessed 2 September 2021).
Schuurmans, Carl C.L., et al., 2021. Hyaluronic acid and Chondroitin sulfate (Meth) Acrylate-Based hydrogels for tissue engineering: synthesis, characteristics and pre-clinical evaluation. Biomaterials 268, 120602.
Shepherd, D.E.T., Seedhom, B.B., 1999. Thickness of human articular cartilage in joints of the lower limb. Ann. Rheum. Dis. 58, 27–34. http://ard.bmj.com/. (Accessed 10 December 2021).
Tsou, Yung Hao, Joe Khoneisser, Huang, Ping Chun, Xu, Xiaoyang, 2016. Hydrogel as a bioactive material to regulate stem cell fate. Bioact. Mater. 1 (1), 39–55.
Valonen, Piia K., et al., 2010. In vitro generation of mechanically functional cartilage grafts based on adult human stem cells and 3D-woven poly(ε-caprolactone) scaffolds. Biomaterials 31 (8), 2193–2200. https://linkinghub.elsevier.com/retrieve/pii/S0142961209013362.
Visser, Jetze, et al., 2015. Reinforcement of hydrogels using three-dimensionally printed microfibres. Nat. Commun. 6 (1), 1–10. www.nature.com/naturecommunications. (Accessed 4 August 2021).
Wilson, W., et al., 2004. Stresses in the local collagen network of articular cartilage: a poroviscoelastic fibril-reinforced finite element study. J. Biomech. 37 (3), 357–366. https://pubmed.ncbi.nlm.nih.gov/14757455/. (Accessed 6 July 2021).
Wilson, W., van Donkelaar, C.C., van Rietbergen, B., Huiskes, R., 2005. A fibril-reinforced poroviscoelastic swelling model for articular cartilage. J. Biomech. 38 (6), 1195–1204. https://wwwsciencedirectcom/science/article/pii/S0021929004003367#fig1. (Accessed 30 October 2018).
Xiao, Yinghua, Friis, Elizabeth A., Gehrke, Stevin H., Detamore, Michael S., 2013. Mechanical testing of hydrogels in cartilage tissue engineering: beyond the compressive modulus. Tissue Eng. B Rev. 19 (5), 403–412. http://online.liebertpub.com/doi/abs/10.1089/ten.teb.2012.0461.
Zhou, Chengjun, Wu, Qinglin, 2011. A Novel Polyacrylamide Nanocomposite Hydrogel Reinforced with Natural Chitosan Nanofibers. Colloids Surf. B Biointerfaces 84 (1), 155–162.